Supercond. Sci. Technol. **13** (2000) R53–R69. Printed in the UK PII: S0953-2048(00)01631-6

TOPICAL REVIEW

Integrated superconducting receivers

V P Koshelets and S V Shitov

Institute of Radio Engineering and Electronics, Mokhovaya 11, 103907 Moscow, Russia

E-mail: valery@hitech.cplire.ru

Received 10 December 1999

Abstract. The concept of a fully superconducting integrated receiver is developed and experimentally tested. This single-chip sub-mm wave receiver includes a planar antenna integrated with a SIS mixer and an internal superconducting Josephson-type local oscillator (flux-flow oscillator, FFO). The receiver is tested with a DSB noise temperature below 100 K around 500 GHz being pumped by its internal local oscillator (LO). The instantaneous bandwidth of 15–20% is estimated via FTS and heterodyne measurements that meet the requirements of most practical applications. The far field antenna beam is measured as $\approx f/10$ with sidelobes below -16 dB that is suitable for coupling to a real telescope antenna. A nine-pixel imaging array receiver with each pixel containing an internally pumped receiver chip is developed and tested. A linewidth of the phase locked FFO as low as 1 Hz is measured relative to a reference oscillator in the frequency range 270–440 GHz. An rf amplifier on the base of a dc SQUID is developed and tested showing a noise figure below 10 K at 4 GHz and a bandwidth of about 300 MHz. This amplifier can be included as a part of an integrated receiver that is valuable for array applications.

1. Introduction

A lightweight and compact ultra-sensitive sub-mm superconducting integrated receiver (SIR) with low power consumption is very attractive for both radio-astronomical research and distant monitoring of the Earth's atmosphere. The new ambitious radio-astronomy multi-dish projects (e.g. ALMA) would gain considerably by using single-chip SIRs due to their lower price and better serviceability as compared to conventional approaches. A distant study of atmospheric pollution is possible using air- or satellite-borne SIRs for detection of the spectrum lines of ozone, chlorine and other elements in the sub-mm wave range. Currently the single-chip superconducting receiver comprises a SIS mixer with a quasioptical antenna and a superconducting local oscillator (LO). In future it could be followed by an intermediate frequency SQUID amplifier and superconducting circuits for digitization of down converted signals and their real time processing. In this review the latest results of an SIR study done in tight collaboration between the Space Research Organization of the Netherlands (SRON-Groningen) and the Institute of Radio Engineering and Electronics (IREE-Moscow) are presented.

A SIS mixer is currently the most sensitive detector element for a heterodyne reception in the frequency range 100–1000 GHz [1–6]. SIS receivers are being used successfully in radio astronomy for observation of spectra showing the lowest noise temperature in the mm and sub-mm wave range. The noise temperature of a SIS receiver is ultimately limited only by the fundamental quantum value $hf/2k$. Since there are many applications lacking a compact and easily tunable sub-mm local oscillator, the direct integration of a superconducting LO with the SIS mixer is a good chance for a serious breakthrough. Two main kinds of superconducting oscillator are under investigation: arrays of the lumped Josephson junction and distributed flux-flow oscillators (FFO).

Several types of Josephson one-dimensional (1D) and two-dimensional (2D) arrays have been proposed and studied [7–18]; most of them are based on overdamped Josephson junctions (JJs) with non-hysteretic current–voltage characteristics (IVCs). Series 1D arrays have been studied for many years; nowadays the most developed design combines compact groups of JJs placed in a microstrip transmission line with a distance of $\lambda_{opt}/2$ [7–12]. A power as high as 0.85 mW has been detected in a matched load at an optimal (resonance) frequency of about 240 GHz [10]. Radiation from the linear array oscillator was measured both by an integrated on-chip detector and by sensors outside the test cryostat. As a rule the maximum operation frequency of the 1D arrays was limited by plasma frequency and the LC resonance frequency of the shunt resistor (typically the maximum operation frequency was about 300 GHz [7–10]). To extend this limit up to 1 THz a new shunted junction with a small parasitic inductance of about 100 fH has been developed [11, 12]. The inductance was minimized by reducing the inductive length between the tunnel junction and a contact hole to about 1 μm. As a result power as large as 10 μW has been delivered to the integrated load at 625 GHz. A composite linewidth of two 1D JJ oscillators of about 8 MHz was measured at 566 GHz. However, a considerable variation of the JJ array output power over the frequency

range makes a direct implementation of the existing JJ array in integrated receivers rather problematic (especially taking into account the absence of an 'internal' mechanism for adjustment of the emitted power). To adjust the output power level, an integrated superconducting attenuator [19] with electronic tuning can be used. This device employs the dependence of a quasi-particle rf current of a SIS junction on the junction bias voltage. Such an attenuator has a frequency range of about 10%, a dynamic range of a few dB (the lower the frequency, the wider the dynamic range) and is limited to a few microwatt saturation level.

Many different designs of the 2D arrays were evaluated [13–18]; some of these demonstrated good frequency tuning—from 100 to 250 GHz at the 3 dB level [17], or very efficient dc/rf power conversion (up to 30% for a 2D array of underdamped JJs [18]). Nevertheless, taking into account all requirements for the superconducting LO for an integrated sub-mm receiver, all developed JJ array oscillators are not matured yet for real applications.

At the moment a flux-flow oscillator (FFO) based on the unidirectional flow of magnetic vortices in a long Josephson tunnel junction [20] looks most developed for integration with a SIS mixer. Local oscillators based on Nb–AlO_x–Nb FFOs have been successfully tested from about 120 to 700 GHz (gap frequency of Nb) providing power sufficient to pump a SIS mixer (about 1 μW at 450 GHz); both the frequency and the power of the FFO can be tuned [21, 22]. A front-end noise temperature of 85 K has been achieved at 140 GHz for a waveguide integrated receiver with an FFO [23]. Recent progress on the development of a quasi-optical integrated receiver with an FFO [24, 25] will be presented in detail in this review; here just few important points are worth mentioning. (i) A receiver DSB noise temperature below 100 K has been achieved for an SIR with the internal FFO operated over the frequency range 480–520 GHz [26]; this means that the performance of the SIS mixer is close to the quantum limit. (ii) An FFO linewidth considerably below 1 MHz has been measured near 450 GHz [27, 28]. Furthermore, recently the feasibility of phase locking the Josephson FFO to an external oscillator has been demonstrated experimentally [28]. An FFO linewidth as low as 1 Hz (determined by the resolution bandwidth of the spectrum analyser) has been measured relative to a reference oscillator in the frequency range 270–440 GHz. (iii) An FFO can be fabricated on the base of the same trilayer (and by using the same technological procedure) as a SIS mixer; the complexity of the FFO circuit is much lower compared to any JJ array oscillator.

Superconducting rf amplifiers ($f_{IF} \sim 100$ MHz) have been realized on the base of dc SQUIDs with noise temperature of about 1 K [29–31]. The most important advantages of an IF SQUID amplifier (SQA) are: (i) its extremely low power dissipation < 1 nW; (ii) small size $\sim$1 mm^2; (iii) full electrical and temperature compatibility with the SIS mixer and FFO. Recently a new design of SQA has been developed for the frequency range of 4 GHz, utilizing a low-capacitance integrated input coil enclosed inside the SQUID loop [30, 32–34]. This design has provided acceptable coupling ($k = 0.6$) under extremely small parasitic capacitance. The following parameters of the two-stage SQA have been measured at the 3.65 GHz: gain of (17.5 ± 1) dB, 3 dB bandwidth of about 250 MHz and noise temperature (4.0 ± 0.5) K [32–34].

A superconducting digital correlator might be used as a backend device for a fully integrated receiver. A proposed concept [35] is based on employing the ultrafast RSFQ elements [36] in the digital sign correlator architecture that is well developed for semiconductor circuitry. The first version of a fully integrated 16-channel RSFQ autocorrelator operating at 11 GHz has been already realized experimentally by Rylyakov *et al* [37].

In this review the main attention will be paid to the results of a comprehensive test of an improved 500 GHz integrated quasioptical receiver comprising an FFO and SIS mixer with planar antenna. The aim of this study is optimization of the chip design and experimental setup in order to achieve the ultimate performance of the receiver. The recent encouraging experimental tests of the dc SQUID based 4 GHz amplifier are discussed. The estimation of the main parameters of the superconducting RSFQ digital correlator is also presented.

2. Properties of the flux-flow oscillators

In the past few years it has been proven that the FFOs [20] can be used as reliable wide-band and easy tunable local oscillators suitable for integration with a SIS mixer in a single-chip sub-mm wave receiver [24–26]. The FFO is a *long* Josephson tunnel junction in which an applied dc magnetic field and a bias current drive a unidirectional flow of fluxons, each containing one magnetic flux quantum, $\Phi_0 = h/2e \approx 2 \times 10^{-15}$ Wb. The symbol h is the Planck constant and e is the electron charge. An external coil or an integrated control line with current I_{CL} can be used to generate the dc magnetic field applied to the FFO. According to the fundamental Josephson relation the junction biased at voltage V oscillates with a frequency $f = (2\pi/\Phi_0)V$ (about 483.6 GHz mV^{-1}). The velocity and density of the fluxons and thus the power and frequency of the emitted mm-wave signal may be adjusted independently by joint action of bias current and magnetic field.

Long Josephson Nb–AlO_x–Nb junctions with overlap geometry are used as FFOs (see the inset in figure 1). The FFO length, L, and the width, W, are about 500 and 3 μm, respectively. The value of the critical current density, j_c, is in the range 2–8 kA cm^{-2} (Josephson penetration depth $\lambda_J \approx$ 8–4 μm), which corresponds to a specific resistance, $R_nLW \approx$ 100–25 Ω μm^2. The values of the London penetration depth $\lambda_L \approx$ 90 nm) and the junction specific capacitance ($C_s \approx 0.08$ pF μm^{-2}) are assumed for the numerical calculations. An active area of the FFO (i.e. tunnel barrier) is usually formed in a long window of the relatively thick insulation layer (200–350 nm, SiO_2) between two superconducting (Nb) films (base and counter-electrodes). The so-called 'idle' region between the overlapping electrodes adjacent to the junction forms a transmission line in parallel to the FFO. The width of the idle region is about the junction width ($W_i \approx 3$ μm) that is limited usually by the alignment accuracy of the fabrication process. One of the electrodes of the FFO is employed as a control line producing the magnetic field, B_{appl}, while the dc current is passing along this electrode.

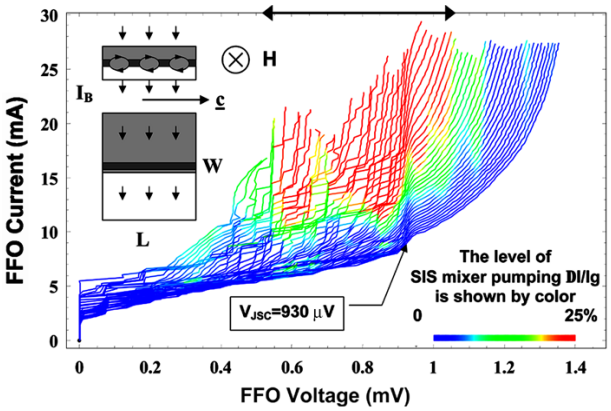

Figure 1. IVCs of the Nb–AlO_x–Nb FFO recorded at different magnetic fields produced by an integrated control line. Note an abrupt changing of the IVC at boundary voltage $V_{JSC} \approx 930\ \mu$V. Inset, cross section of the long junction with driven vortices (top) and its layout (bottom). Here I_B is bias current; L and W are length and width of the FFO respectively.

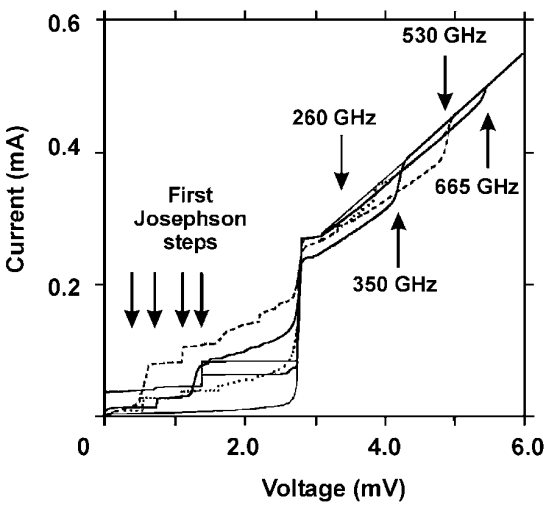

Figure 2. IVCs of the SIS detector (wide band design) pumped by an FFO at different frequencies [21]. The arrows are pointing to quasi-particle (tunnel-assisted) steps and first Shapiro steps for frequencies 260, 350, 530 and 665 GHz.

2.1. Frequency and power tuning

To characterize an FFO as an rf source, a special integrated circuit comprising a well coupled wide-band SIS detector is used. A typical set of the current–voltage characteristics (IVCs) of the FFO (measured at different magnetic fields) is shown in figure 1. Simultaneously with recording of the FFO IVCs, the pump of the integrated SIS detector was measured by an IRTECON system (see below). The voltage range where the FFO delivers sufficient power to pump the integrated SIS detector is marked on the top voltage axis in figure 1. The criterion of a good pump is the change of the subgap tunnel current of the SIS detector at $V = 2$ mV due to photon assisted tunnelling, ΔI, compared to the current rise at the gap voltage I_g. A ratio $\Delta I/I_g$ more than 0.25 is realized for the FFO voltages from 550 to 1070 μV (see figure 1) that corresponds to the frequency range 270–520 GHz. The IVCs of the SIS detector recorded at different setting of the FFO are shown in figure 2 [21]. Well pronounced quasiparticle steps

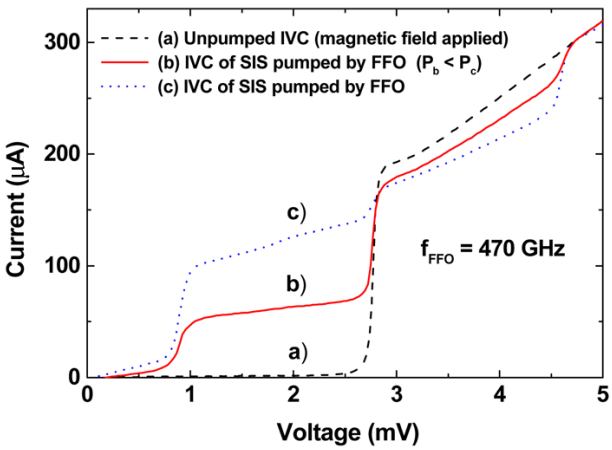

Figure 3. IVC of the SIS mixer: a, without FFO pumping; b and c, pumped by the FFO at 470 GHz for two levels of the FFO power (explained in the text) [39]. The ac Josephson effect is suppressed by current through the integrated control line.

are clearly visible on the SIS IVC up to an FFO frequency of 665 GHz. Actually the frequency operation range is limited by matching circuits and SIS tuning structure rather than the FFO itself. It is possible to considerably change the operation range of the integrated circuit by modifying the design of the matching elements. An implementation of the FFO based on superconductors with a higher critical temperature (higher gap voltage) results in considerable increase of the operation frequency; recently an excitation of the resonances by Josephson radiation at frequencies up to 1.5 THz have been demonstrated [38] for NbN and NbC_xN_{1-x} tunnel junctions.

Since the power and frequency of the emitted mm-wave signal may be adjusted independently, the FFO power can be precisely tuned at a fixed frequency. The curve 'a' in figure 3 [39] shows the autonomous SIS IVC—without FFO pumping. The Josephson effect in the SIS junction is suppressed by dc current through the integrated control line made in one of the electrodes of the junction. The IVCs of the SIS mixer pumped by the an FFO operating at $f = 470$ GHz for two different power levels are presented by curves 'b' and 'c'. The normalized RF voltage, $\vartheta = eV_{RF}/hf$ ($\vartheta_b \approx 1.1$, $\vartheta_c \approx 1.9$) is estimated by fitting the numerically simulated IVCs to the measured ones. From figure 3 one can see that the power provided by the FFO is sufficient to operate a SIS mixer; this power can be continuously adjusted over a range of about 10 dB.

2.2. Regimes of the FFO operation

Study of long Josephson junctions intended for wide band integrated oscillators was performed in detail [40]. Zero field steps (ZFSs) in the IVC of the FFO were observed for small magnetic fields. The position of the ZFS is dependent on length and propagation velocity of the electromagnetic wave along the FFO. The so-called Swihart velocity, c_{Sw}, is the maximum velocity of fluxons in the junction. The 'idle' region in parallel to the junction has a much higher propagation velocity than that of the bare Josephson transmission line. This results in an increase of the effective Swihart velocity c_{Sw}^{eff} and consequently, the voltage

of the ZFS, V_{ZFS}, is significantly increased. The value of c_{Sw}^{eff} depends [41] on the ratio W_i/W and, using the parameters stated above, is about 1.3 c_{Sw}.

The so-called displaced linear slope (DLS) is observed in the IVC of the FFO at low magnetic fields. With increasing B_{appl} (see figure 1 at $V < 400\ \mu$V) the DLS branch shifts almost linearly with B_{appl} towards higher voltages. When the FFO is biased within the DLS region, instead of the usual distinct superposition of quasi-particle and Shapiro steps, a 'smearing' of the IVC of the SIS detector at $V \approx 0$ and $V \approx V_g$ was found [40]. This means, most probably, that the FFO operates as a wide-band noise source while biased at DLS. Such behaviour was reported for the first time in a recent paper [42], where an extremely broad radiation linewidth was observed for an FFO biased at the DLS. Numerical simulations [42] showed that the FFO dynamic at DLS is characterized by irregular fluxon oscillations that resemble a chaotic state. Qualitatively, the complicated fluxon dynamic can be attributed to excitation of the internal oscillation modes in the 'soft' fluxon chain at weak magnetic fields.

The DLS transforms into the flux-flow step (FFS) at higher magnetic field; the FFS subsequently splits [43] into a series of resonant Fiske steps (FSs) that is clearly seen in figure 1. This resonant mode takes place up to a specific 'boundary' voltage, V_{JSC}, where the FSs merge into the Eck peak. At the same voltage, V_{JSC}, a 'bump' in dc current appears. As also seen from figure 1 for $V > V_{JSC}$, the FFS becomes smooth and with increasing magnetic field it persists up to the gap voltage. It should be noted that this 'boundary' is typical for all investigated FFOs with high current density ($j_c > 1\,\mathrm{kA\,cm^{-2}}$). This feature does not depend significantly either on the exact junction geometry and its dimensions or on the coupling to the external microwave circuits.

The boundary voltage is about one third of the superconductor gap voltage; that is $\approx$950 μV for Nb–AlO_x–Nb tunnel junctions. To explain the experimentally measured I–V curves, a model based on self-coupling of Josephson radiation was introduced [40]. The effect of Josephson self-coupling (JSC) [44] is basically absorption of ac radiation by the quasi-particles in the cavity of the long junction. It is very much related to the well known phenomenon of photon assisted tunnelling. The JSC results in current bumps (similar to quasi-particle steps in a SIS mixer) at $V_{JSC} = V_g/(2n+1)$, which gives $V_{JSC} = V_g/3$ for $n = 1$. The effect of self-pumping explains not only the current bumps observed in the FFO I–V curve, but also the abrupt merging of Fiske steps (absence of resonant mode at $V \geqslant V_g/3$). That is caused by increase of the internal damping in the long junction due to quasi-particle tunnelling [40]. In other words, the geometric resonances (or FSs) may exist only for low normalized damping, $\alpha l < 1$ (where $l = L/\lambda_J$ is the junction length normalized to the Josephson penetration length λ_J). It worth to note that the resonant conditions can be satisfied even for a very long junction, $l = L/\lambda_J \geqslant 100$, if the damping is sufficiently low (say, $\alpha \leqslant 0.01$). According to theory, the FSs transform into the so-called Eck peak when the normalized damping increases to a value of about $\alpha l \geqslant 2$. This threshold depends on both length and initial damping. In accordance with qualitative calculations [40] the damping parameter becomes five times as large for $V > V_{JSC}$ and an FFO enters the 'real' flux-flow regime with a possibility of permanent frequency tuning by the magnetic field.

3. FFO linewidth; phase locking to an external oscillator

The frequency resolution of a receiver (along with the noise temperature and the antenna beam pattern) is one of the major parameters in spectral radio astronomy. The resolution is determined by both the instant linewidth of the local oscillator and its long-time stability; it should be much less than 1 ppm of the centre frequency. Previous measurements on the linewidth of the FFOs [21, 45–48] have demonstrated the following values: 130 KHz at 70 GHz [45], about 1 MHz at 280 GHz [21, 46] and 2.1 MHz at 320 GHz [47]. Recently linewidths considerably below 1 MHz have been measured near 450 GHz [27]. Unique time resolved measurements of FFO radiation were performed by using an acousto-optical spectrometer (AOS) with an integration time of 1 μs; a linewidth of a free-running FFO less than 1 MHz at 350 GHz has been demonstrated [48]. However, the observed FFO linewidth is almost one order of magnitude wider [21, 46] than predicted by the theory for a lumped Josephson tunnel junction.

3.1. Linewidth of the FFO

Currently no reliable theory exists for the FFO linewidth, but preliminary estimations [49] have been done on the basis of the general theory for the radiation linewidth of the *lumped* Josephson tunnel junction [50]. The linewidth, Δf, of a Josephson junction is mainly determined by low frequency current fluctuations. For white noise it can be written (see e.g. [51]) as:

$$\Delta f = (2\pi/\Phi_0^2)(R_d^B)^2 S_i(0) \tag{1}$$

where $S_i(0)$ is the density of the low frequency current fluctuations, $R_d^B = \partial V/\partial I_B$ is the dc differential resistance which transforms the current fluctuations to voltage (and phase) noise. For a lumped tunnel junction [50, 51]

$$S_i(0) = (e/2\pi) I_B(V_{dc}) \coth(v) \quad \text{with } v = (eV_{dc})/(2k_B T_{eff}) \tag{2}$$

where k_B is Boltzmann's constant. I_B and V_{dc} are the current and averaged dc voltage at the bias point. T_{eff} is the effective temperature of the quasiparticles in the junction electrodes. These formulae describe a nonlinear superposition of thermal and shot noise. It should be noted that the formulae (1), (2) do not take into account the spatial variation of the tunnel current along the FFO, the interactions of the moving fluxons and the influence of the external low frequency interference. All these effects are believed to increase the FFO linewidth.

Fluctuations in the external magnetic field can be accounted for by the differential tuning resistance of the control line $R_d^{CL} = \partial V_{FFO}/\partial I_{CL}$ for fixed dc bias current I_B. In the case of *external interference* both the 'usual' differential resistance R_d^B and R_d^{CL} 'convert' low frequency external noise currents, $I_{lf}^{(B,CL)}$, to frequency fluctuations following the same relations:

$$\Delta f \propto R_d^{(B,CL)} I_{lf}^{(B,CL)}. \tag{3}$$

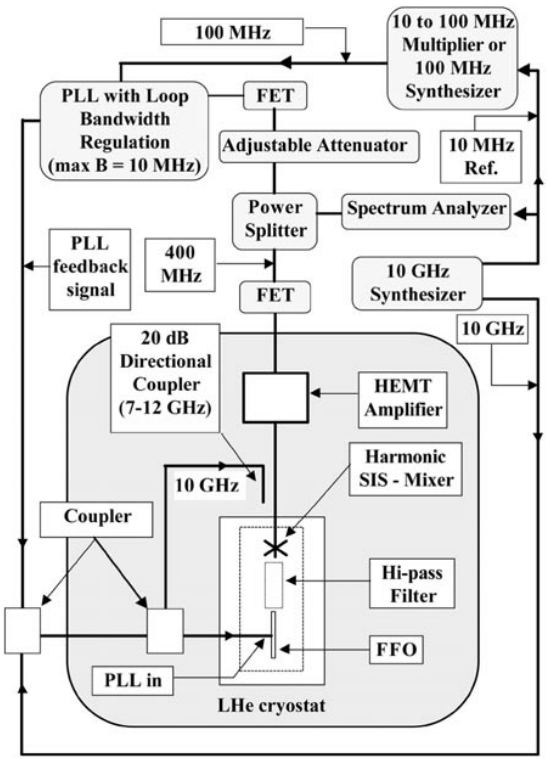

Figure 4. Block diagram of the PLL circuit and set-up for linewidth measurement [49]. The central components are the cryogenic chip with the FFO and SIS mixer, the cooled low noise 400 MHz HEMT IF amplifier and the 10 GHz synthesizer, which also provides a 10 MHz reference signal for the spectrum analyser and the PLL phase detector.

According to this theoretical consideration the radiation linewidth is determined by both the noise level and the differential resistance of the FFO at low frequencies, $f < \Delta f_{AUT}$, where Δf_{AUT} is an autonomous FFO linewidth. Since the FFO is a perfect voltage-controlled oscillator, one can assume that the FFO linewidth can be changed (stabilized) by an external phase-lock loop (PLL) which bandwidth is larger than Δf_{AUT}.

3.2. Experimental setup

A specially designed integrated circuit comprising the FFO, the SIS mixer, and elements for rf coupling, is used for linewidth measurements. Both the SIS and the FFO junctions are fabricated from the same Nb–AlO_x–Nb trilayer; details have been described elsewhere [27, 40].

A block diagram of the set-up for linewidth measurements is shown in figure 4. The FFO linewidth was measured within a wide frequency range up to 600 GHz using a new experimental technique [27]. The signal from the FFO is applied to the harmonic mixer (SIS mixer operated in Josephson or quasiparticle mode) along with the signal from the frequency synthesizer f_{SYN} (about 10 GHz). To prevent the signal of the synthesizer (as well as its low harmonics) from reaching the FFO a high-pass microstrip filter with a cut-off frequency of about 200 GHz is inserted between the FFO and the harmonic mixer. The intermediate frequency (IF) signal with frequency, $f_{IF} = \pm(f_{FFO} - nf_{SYN})$ is boosted

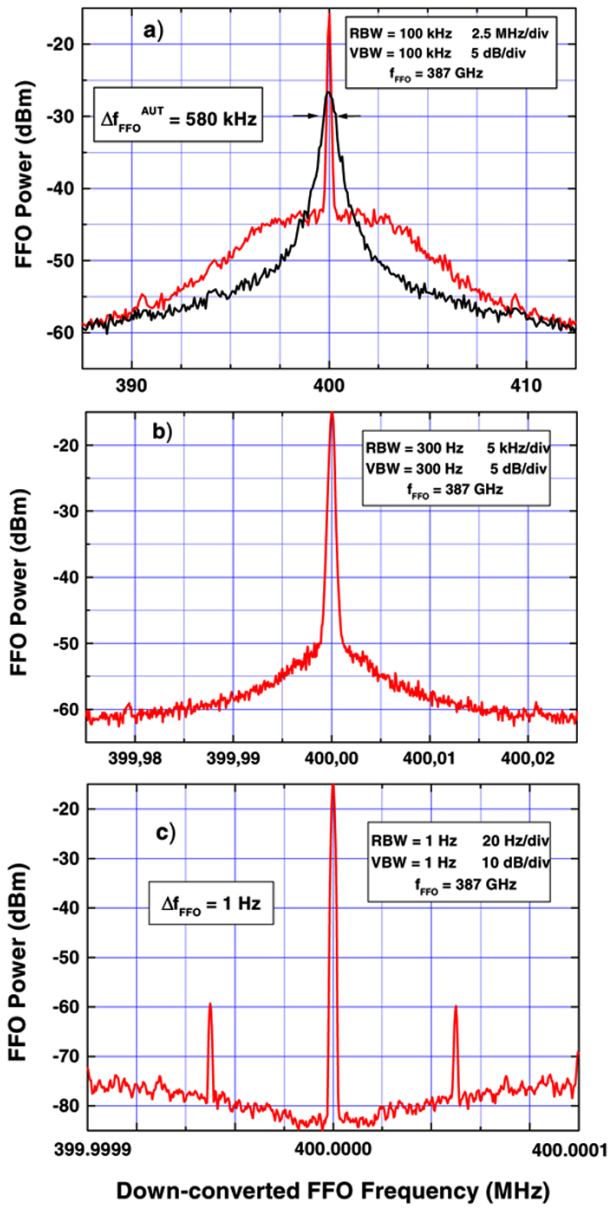

Figure 5. The down-converted IF power spectra of the FFO ($f = 387$ GHz) recorded with different frequency spans clearly demonstrates the phase locking [28].

by a cooled amplifier ($T_n \approx 20$ K, gain= 27 dB) and then by a room temperature amplifier for further use in the PLL system. A part of the signal is applied via the directional coupler to a spectrum analyser which is also phase locked to the synthesizer using a common reference signal at 10 MHz. This down-converted spectrum of the FFO is presented in figure 5. Thus, the spectrum obtained at about 400 MHz, as well as the phase noise evaluated from these data, is a difference between the FFO signal and the nth harmonic of the synthesizer.

In the PLL unit the $\mathrm{IF}_{PLL} \approx 400$ MHz is divided by four and compared in a frequency–phase discriminator with a 100 MHz reference signal (also phase locked to the main 10 GHz synthesizer). The output signal proportional to the phase difference is returned via the loop bandwidth regulator (maximum bandwidth about 10 MHz) and then fed back to the

FFO via a coaxial cable terminated with a cold 50 Ω resistor mounted on the chip bias plate. To reduce the number of wires entering the cryostat, the same coaxial cable is used both for the 10 GHz synthesizer signal and for the feed-back PLL current.

In order to perform accurate linewidth measurement of the free-running FFO, the IF spectra have to be averaged with a sufficiently narrow video bandwidth. The PLL system with a relatively low loop gain and narrow bandwidth setting (< 10 kHz) can be used for *frequency locking* of the FFO in order to measure an autonomous linewidth, Δf_{AUT}, of the free-running FFO. In this case it is assumed that only low frequency noise and drifts are eliminated by the narrow band feedback. Thus the linewidth, determined by much faster fluctuations, which is assumed to be the 'natural' ones, can be carefully measured.

3.3. Results and discussion

Recently the feasibility of phase locking the Josephson FFO to an external reference oscillator has been demonstrated experimentally [49, 28]. It was found experimentally that the PLL system can considerably narrow the FFO linewidth if Δf_{AUT} (measured at the -3 dB level) is smaller than the PLL regulation bandwidth, B_{PLL}. Figure 5 shows typical IF power spectra of the phase locked FFO measured at $f_{FFO} = 387$ GHz for different settings of the spectrum analyser. An FFO linewidth as low as 1 Hz is presented in figure 5(c) being limited by the resolution bandwidth of the spectrum analyser. This experimental fact means that the FFO linewidth can be reduced below the value determined by the fundamental shot and thermal fluctuations of the free-running tunnel junction.

A consequence of the phase locking is the appearance of a vertical step ($R_d^B = 0$) in the dc current–voltage characteristic (IVC) of the FFO at the voltage corresponding to the frequency f_{FFO} where the FFO is locked, see equation (1). The position of this step is insensitive to small changes in the control line current, that means also $R_d^{CL} = 0$. A hold-in range of the FFO voltage as large as 1.5 μV has been experimentally measured. This corresponds to an effective PLL regulation band of about 750 MHz. It should be noted that this vertical step is not a harmonic Shapiro step. First, it is shifted from the position of a possible Shapiro step by 0.8 μV that corresponds to the PLL input frequency of 400 MHz. Furthermore, the position of the vertical step was being tuned precisely by changing the reference signal. The reference signal in the range 90–110 MHz was applied from a second synthesizer phased locked to the first one (see figure 4) in steps of 0.1 Hz (minimum increment of the synthesizer). This corresponds to a voltage accuracy of 2×10^{-16} V.

The residual phase noise of the phase locked FFO (measured relative to the reference synthesizer) is plotted in figure 6 (data from figure 5) as a function of the offset from the 400 MHz carrier. The specification and measured data for the used synthesizer (HP83752B) are shown in figure 6 as well. The FFO was locked to the 36th harmonic of the synthesizer at this measurements, and, to obtain the real FFO phase noise, one should add to the measured residual FFO phase noise the synthesizer noise multiplied by $n^2 = 1296$ as shown in figure 6.

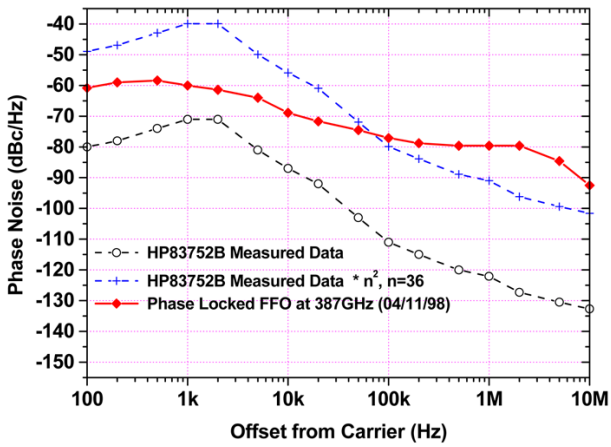

Figure 6. Experimentally measured phase noise of the phase locked FFO at 387 GHz compared with the data for an HP83752B synthesizer [28]. Since the residual phase noise of the FFO is measured relative to the 36th harmonic of the synthesizer, a multiple factor of $36^2 = 1296$ has to be used to estimate the total FFO phase noise.

It should be noted that phase locking of the FFO has been realized only on the steep FSs, where the free-running FFO linewidth is about 1 MHz, associated with the small values of R_d^B and especially R_d^{CL}. An increase of the FFO linewidth has been found at voltages above the boundary voltage, V_{JSC}, [40], where the IVC of the FFO is modified as a result of the abrupt increase of internal damping due to Josephson self-coupling. It is still an experimental challenge to obtain phase locked operation of the FFO in the 'true' flux-flow regime where the normalized damping $\alpha L/\lambda_J \geqslant \pi$ and initial autonomous FFO linewidth is about 10 MHz. For operation at all FFO voltages including $V > V_{JSC}$ additional efforts should be undertaken to decrease the dynamic resistance and thus the initial FFO linewidth. Also an ultra-wide band PLL system with sufficiently low phase noise is needed. In this context the ongoing development of an on-chip integrated phase detector looks promising. The PLL bandwidth in this case will not be limited by the electrical properties of the long interconnection cables. The cryogenic phase detector, low noise amplifiers etc can be constructed using existing superconducting electronic components.

4. Integrated receiver

4.1. Layout of chip receiver

The integrated receivers for the sub-mm wave range (400–700 GH) [24, 26, 52, 53] are fabricated from an Nb/AlO$_x$/Nb trilayer ($j_c \approx 5$ kA cm^{-2}) [54] on a 2 in silicon wafer (0.5 mm thick) and then diced into chips of 4 mm $\times$ 4 mm. A double-dipole antenna SIS mixer [55] is placed in the geometrical centre of the chip where the incoming rf signal is focused by a coated silicon microwave lens [56, 57]. The FFO based local oscillator (LO) is placed just outside the two-wavelength 'hot' spot of the antenna and connected to the mixer with a microstrip transmission line, which contains a number of rf coupling and dc blocking elements. Both the SIS mixer and FFO are provided with local magnetic fields via integrated control lines [24]. All receiver elements are placed in an area

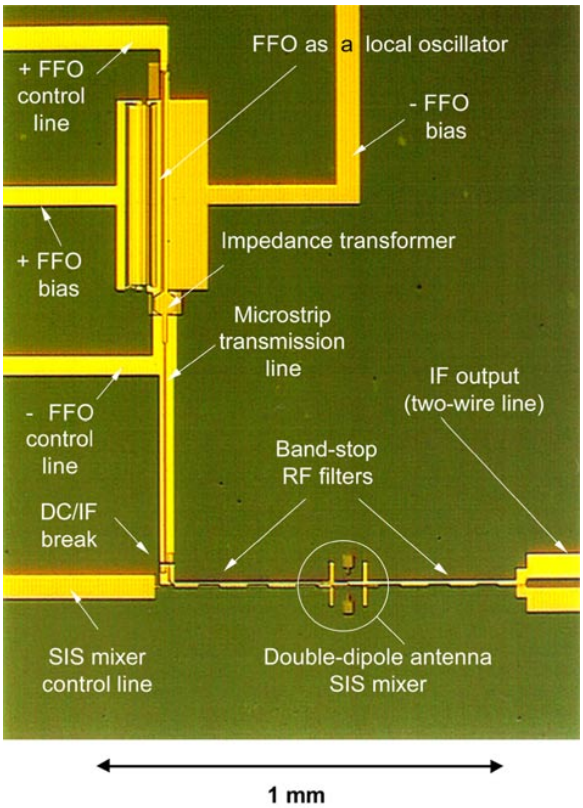

Figure 7. Microphotograph of a central part of the silicon chip of sizes 4 mm by 4 mm. All main elements of the integrated receiver are presented; the back reflector is not yet installed on the double-dipole antenna. Some details of wiring and contact pads are out of the field of view, which is about 1 mm by 1.5 mm.

of about 1 mm × 1 mm, but the chip dimensions are defined mainly by the size of contact pads which were chosen to be about 0.8 mm for easier connection; 11 contact pads are provided for bond-wiring. Two photographs of the chip and a simplified electrical diagram of the receiver are shown in figures 7–9 respectively [53].

4.2. Antenna-mixer design

The concept of a single-junction double-dipole antenna SIS mixer was chosen [55]. This kind of planar integrated lens antenna is compact, although it has to use a back reflector to achieve a beam of good symmetry. The reflector is a quarter-wave thick silicon chip (800 μm × 800 μm) one-side covered with a film of Nb. The double-dipole antenna against the back reflector is treated as a four-dipole array immersed in a silicon medium ($\varepsilon_r = 11.7$). Because of the homogeneity of the medium surrounding the antennas, analytical formulas for a thick wire dipole antenna are used to estimate the main properties of the real device (e.g. feed-point impedance and beam shape). The beam inside the silicon media was estimated taking into account the mutual interference of all four antennas [58]. The calculated main lobe was found to be consistent with the results [55–57] obtained via the momentum method.

A microphotograph of the double-dipole antenna SIS mixer is shown in figure 8 [53]. The mixing SIS junction

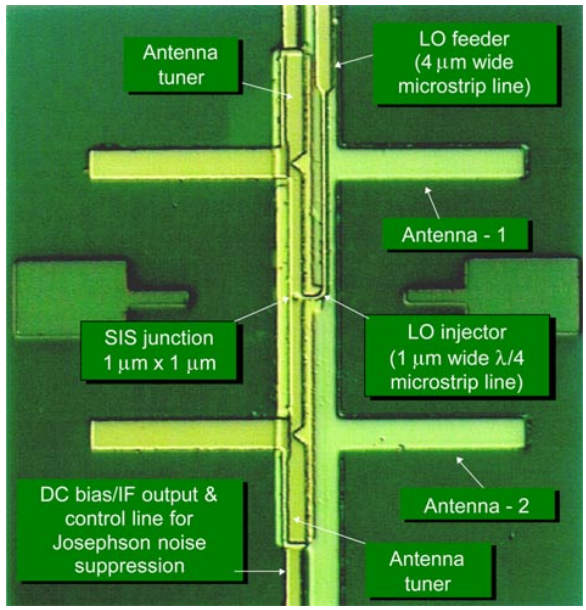

Figure 8. Microphotograph of a double-dipole antenna SIS mixer of the integrated receiver. Microstrip tuners for the antenna and a feeder of the local oscillator are shown. The field of view is about 100 μm by 150 μm.

(1–1.5 μm^2 area) is placed in the centre of the antenna array and connected to both antennas with microstrip transmission lines as a shared load. To improve rf coupling and achieve low noise performance of the mixer, the capacitance of the tunnel SIS junction is tuned out within a certain frequency range around 500 GHz. Each microstrip feeder, connecting the junction to the antenna, is employed as a microstrip tuner for the half-junction while the antenna is tuned with an additional open-end microstrip stub. To supply a localized magnetic field to the SIS junction, the microstrip feeders are used in series forming a common control line. Since a narrower strip can, for a given current, produce stronger magnetic field, the width of 3 μm was chosen in the vicinity of the junction. This width applies a limit for the fabrication misalignment, which is less than 1 μm.

4.3. LO coupling circuit

The FFO of size 450 μm × 4 μm is employed as a local oscillator. Since the frequency of a Josephson oscillator has a fundamental relation with the dc voltage across the junction, the integrated LO has been tested for its tuneability via measuring a dependence of the FFO bias voltage on control line current while the bias current was kept constant. The experimental data obtained with the receiver showed almost linear behaviour (permanent tuneability) in the flux-flow regime from about 500 GHz up to 700 GHz. To couple the power from the FFO, which is basically a Josephson transmission line with an estimated characteristic impedance of about 0.4 Ω [59], to a narrow microstrip transmission line, a special impedance transformer is used. This two-stage tapered transformer was synthesized empirically as a stair-shaped microstrip. The power transmission line is a superconducting microstrip about 900 μm long and 4 μm wide (characteristic impedance of about 14 Ω). To bias

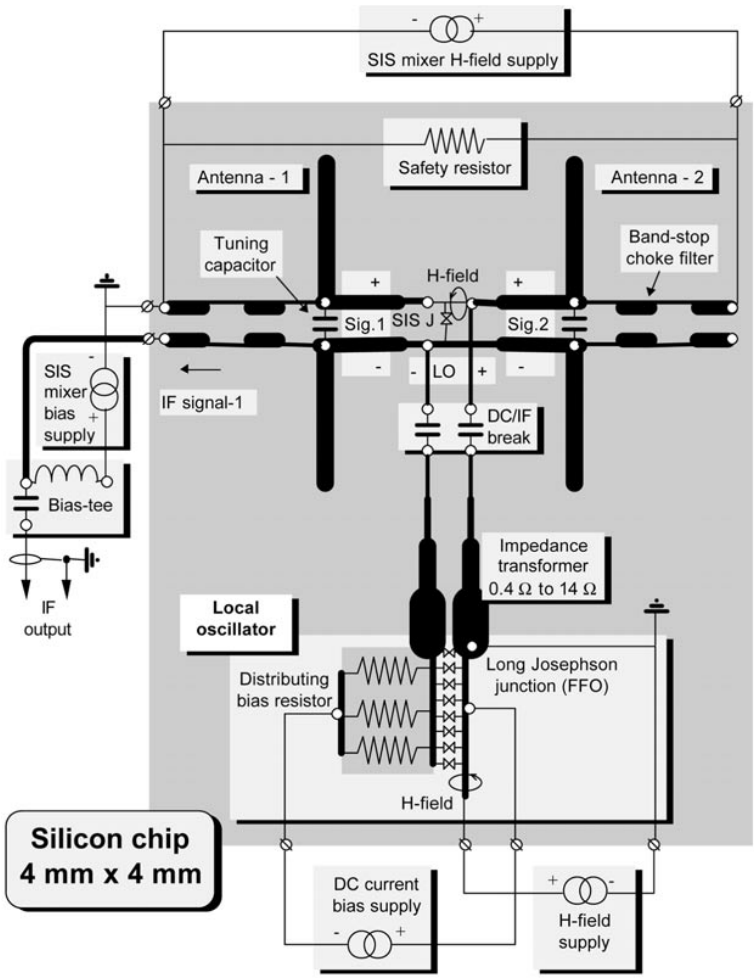

Figure 9. Simplified equivalent diagram of the integrated receiver chip and its external connections. A dc power consumption of the chip is defined by the FFO that is about 20–40 μW.

the FFO and the SIS junction independently, a dc break in both leads [60] is inserted about half way between the LO and the mixer (figure 7). The distant end of the LO path is shaped as a 1 μm wide microstrip, as shown in figure 8, which is a quarter-wave transformer providing the LO output impedance of about 60 Ω in parallel to the mixing junction. This value of impedance is chosen to intently limit the coupling between the mixer ($R_n \approx 20$ Ω) and the LO to about 20–30% to avoid signal loss to the LO path. The power coupled from the FFO to the mixer is shared between the SIS junction and antennas; the last part is lost into emission. It is important to note that the signal loss at the input of the mixer is in direct proportion with the LO coupling efficiency. To estimate the signal loss, a reference SIS mixer has been developed. This device contains the same antenna mixer, but does not have the FFO and the related LO injection circuit. Both smaller disturbance to the antenna beam and lower noise temperature compared to the integrated receiver are measured for this device.

4.4. Optics design

An elliptical silicon lens (truncated ellipsoid $R_1 = 5$ mm, $R_2 = 5.228$ mm) is designed to be the only optical element providing a diffraction limited beam $f/10$ at 450–550 GHz [56, 57]. To improve the beam coupling via reducing reflection at the silicon–vacuum interface, an antireflection coating (87 μm thick) made from Stycast 1264 epoxy ($\varepsilon \approx 2.9$) is applied to the lens. Both the lens and its antireflection layer have been fabricated by diamond turning with surface accuracy better than 5 μm. The chip is installed on a flat back of the lens using paraffin wax or a soft '3M' 2216 epoxy in such a way that the antenna is, within an accuracy of ± 10 μm, in the focus of the lens. A printed circuit board (PCB), which provides mechanical support for dc and IF connections, presses the lens down against a cold (about 4.2 K) copper block installed in the vacuum space of the optical cryostat with liquid helium (see figure 10).

4.5. Shielding

It is worth recalling that the FFO is a magnetic sensitive device. For this reason a special shielded setup has been developed that is presented schematically in figure 10. The shielding inside the cryostat is provided by two coaxial cans with an external layer made from cryo-perm and an internal one made from copper covered with 100 μm of superconducting led. A thermal coupler made from copper

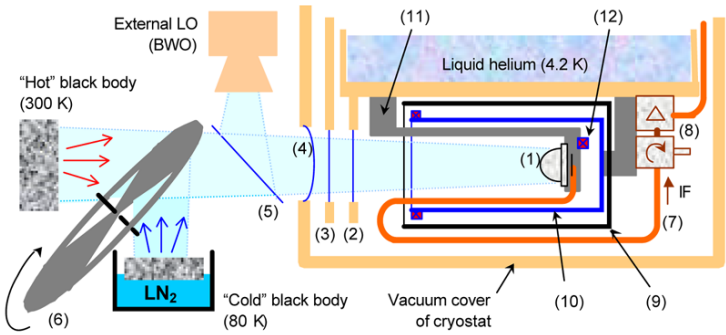

Figure 10. Schematics of experimental setup including details of beam coupling, interior of cryostat and magnetic shielding: (1) silicon elliptical lens with antireflection coating; chip receiver is glued at its flat back, (2) Zitex infrared filter at 4.2 K, (3) resonant plate filter of Teflon or quartz at 80 K, (4) resonant vacuum window of Mylar or Kapton, (5) thin film beamsplitter (not used with internal LO), (6) chopper wheel switching 'hot' and 'cold' antenna loads ($f_{chop} \approx 11$ Hz), (7) semirigid coaxial IF cable, (8) shielded IF isolator and 30 dB IF amplifier (1.3–1.8 GHz), (9) external shielding layer (μ-metal), (10) internal superconducting shield, (11) holder (heat sink, the 'leg') of copper, (12) heaters for chip and superconducting shield.

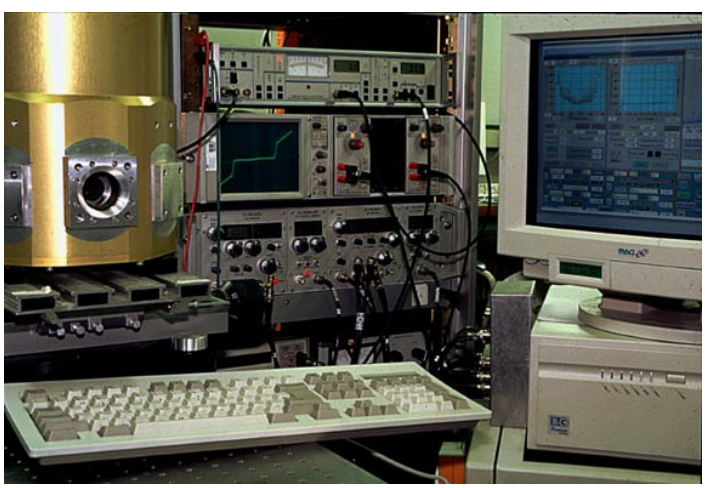

Figure 11. Photo of the experimental set-up controlled with the IRTECON system: quasi-optical cryostat on the left, bias supply unit in the centre (in the background) and data display on the right.

(the 'leg') is holding the chip far enough from the opening of the shielding can which is the only aperture for entry of the signal beam and all electrical connections. The superconducting shield can be heated up to remove trapped magnetic flux. The shield and the 'leg' are thermally isolated from each other having independent heat contacts to the bottom of the liquid helium bath. To reduce risk of flux trapping in the shield, a *magnetically shielded* ferrite isolator is used at the input of the IF amplifier. The shield was tested qualitatively with a strong constant magnet (about 2000 G in the gap of 5 cm between poles) moved around at 5 cm distance from the opening of the shield (near the cryostat window). A voltage shift of about 2 μV was detected at the FFO at fixed bias current; a suppression factor of about 10^{-4} has been estimated. The cross-talk between control lines of the SIS mixer and FFO was also measured and found to be at a level of about 10^{-3}.

4.6. Data acquisition system IRTECON

From figure 9 one can see that the chip of the integrated receiver needs four floating bias sources. It was recognized easily that manual control of the chip is very slow and far not effective even for a brief test. A data acquisition system for the integrated receiver test and control (IRTECON) was developed for automatic collection of dc and rf data [53]. The basic system includes an analogue bias supply, designed as a standard 19-inch rack, and a controlling computer. The controlling computer is equipped with two acquisition cards from National Instruments: a 16-bit resolution card for the FFO and a 12-bit resolution card for the SIS mixer. Four DACs and ten ADCs are used in the system to hook up the analogue bias supply, the rf detector and the lock-in amplifier. The software package is written under 'LabWindows' in such a way that it can be configured for a wide range of experiments. The general view of the setup is presented in figure 11.

The IRTECON measures I–V curves of both the FFO and SIS mixer and allows visualization of the pump level of the mixer in a quasi-colour. The blue colour (of the rainbow palette) on the I–V curve of the FFO corresponds to the dark current of the mixer (i.e. no pump) while the red colour is associated with a threshold behind which the pump (i.e. photon-induced current in the mixer) is sufficient for the optimal heterodyne reception. The size and position of the red region is a qualitative, but very convenient visual datum.

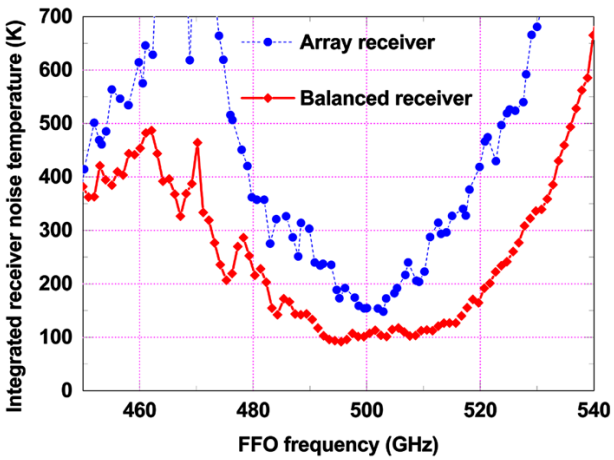

Figure 12. Circles, experimental data on a typical single-junction pixel pumped by its internal FFO in a nine-pixel array cryostat. The data are collected automatically by the IRTECON system; ripples are associated with interference on a thick 80 K infrared filter. Diamonds, data on a pixel with the double-junction *balanced SIS mixer* pumped by the integrated FFO measured in a smaller test cryostat.

Setting the FFO at the centre of this region, one can obtain about the maximum available pump.

One of the most advanced routines is optimizing the receiver noise temperature, T_{RX}, within a particular frequency range via selection of both the optimum pump level and the best bias point for the SIS mixer. The LO power supplied to the SIS mixer is varied via FFO bias current while the LO frequency is kept constant by adjustment of magnetic field (i.e. via control current of the FFO). The Y factor is measured at IF $\approx$ 1.5 GHz with a fast rf detector, lock-in amplifier and running 'hot/cold' chopper (see figure 10). Since the traces of T_{RX} against mixer bias usually are *not* crossing each other, the lowest noise figure is assumed belonging to the lowest curve. This means that the optimum pump level can be found using any reasonable bias voltage, V_{SIS}, within the range of about 1–2.5 mV. In the following step an optimization of the receiver noise temperature on the SIS mixer bias voltage takes place. The described routine is intended for finding and long term tracking of the (static) regime of the receiver.

IRTECON is a quite flexible tool. For example, the data on receiver noise temperature presented in figure 12 are taken in a quite different (dynamic) regime of fast sweeping all possible settings of the FFO at selected settings of the SIS mixer. This allows us to obtain the desired 'density' of the data which have then to be processed (filtered) for finding the best response (the lowest noise temperature) at each FFO frequency.

Two main sets of measurements are performed: (i) a preliminary dipstick test at dc (no signal applied to the antenna); (ii) a real receiver test in a vacuum cryostat with an optical window. I–V curves for both the SIS mixer and the FFO, as well as the pump level and its range are the data obtained via the first test. Since no *external* magnetic field is allowed to operate the chip receiver, the suppression of a Josephson current in the SIS mixer by the integrated control line is usually the first datum one has to measure qualifying the chip. A control line current of about 30–40 mA is usually enough to provide the first minimum for a 1.5 μm^2 junction, while the control line can withstand current more than 150 mA. The maximum LO power, measured in the dipstick, is usually in the range of 50–100 nW at about 500 GHz, that is estimated via a pumped I–V curve of the SIS mixer. The complete *test* run (i.e. preliminary selection) takes about 45 minutes per device including mounting into the dipstick and printing selected data.

The second test routine is split in three stages: (i) a Fourier transform spectrometer (FTS) test gives an instantaneous bandwidth of the mixer in a video-detection mode; (ii) a hot–cold test in the heterodyne mode gives the receiver noise temperature and the available bandwidth; (iii) an antenna beam test concludes the characterization of the device for a real application. The FTS tests confirmed that the mixer is properly tuned around 500 GHz and instantaneous video bandwidth is about 60–70 GHz.

4.7. Noise temperature and antenna beam pattern

Figure 12 presents typical data on the double-side band (DSB) noise temperature obtained with internal LO for two types of chip receiver: a single-junction SIS mixer (circles) [24] and balanced SIS mixer (diamonds) [52]. Data in an array cryostat are not corrected for any additional loss associated with this arrangement (see section 5 below). Data for a balanced receiver are measured in a smaller cryostat intended for a single device test. This basic arrangement is presented in figure 10. Noise figures measured for a device in the small test cryostat are usually about 10–20% lower for reasons discussed below.

It is always a point of interest to compare the operation of the chip receiver with internal and external local oscillators using the general setup presented in figure 10. It was found that, outside the region of best sensitivity, the noise temperature can be somewhat higher in the case of an internal oscillator that is associated with lack of LO power. Another FFO related effect was detected for the fraction of the range close to 480 GHz—poor operation of the FFO caused by proximity to the boundary voltage. As explained above, there is no possibility for permanent tuning of the FFO frequency below the boundary voltage and FFO IVCs are very steep just above it. That is why the heterodyne data on most integrated receivers designed for the 450–550 GHz band lack good response near 480 GHz while a much wider bandwidth is obtained via FTS test or with an external LO.

On the base of noise contribution analysis done by Baryshev *et al* [61] it became possible to reduce the receiver noise temperature below 40 K at 475 GHz for a reference SIS mixer pumped by an external LO. This is, to the authors' knowledge, the lowest value reported within this frequency range. It worth mentioning that the noise analysis for the reference receiver [61] does not show any considerable unknown noise contribution. The additional difference in the noise temperature of a SIR compared to a reference receiver is due to some modifications in the measuring setup: (i) a very thin 15 μm Kapton window instead of 175 μm Mylar; (ii) shorter IF cables with an additional thermal sink between

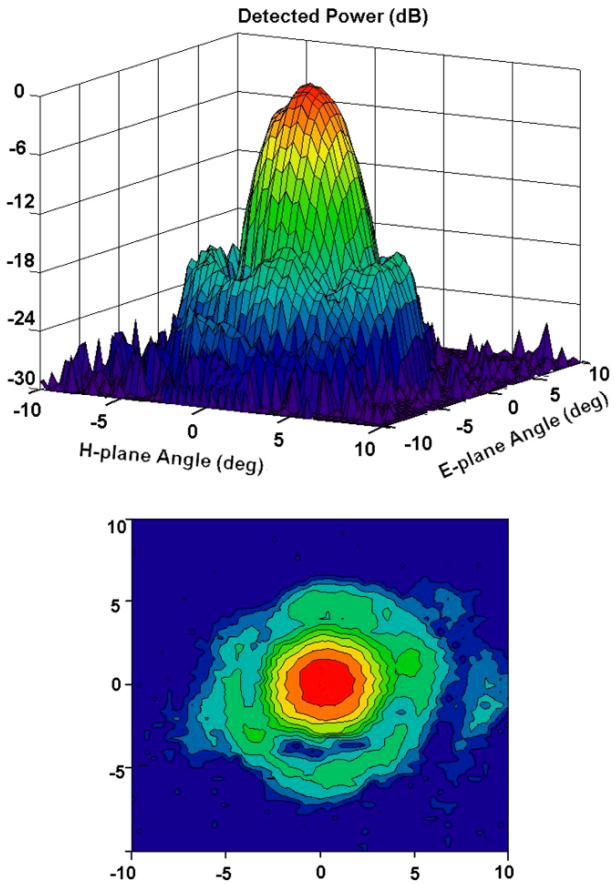

Figure 13. Antenna beam pattern of the SIR pixel measured at the distance of 400 mm from the cryostat window at 490 GHz. Data for the raster image are collected from an area 100 mm by 100 mm. The equal power contours are placed with steps of 3 dB. The first sidelobe is found at −16 dB. Some asymmetry is assumed to be a result of sidelobes touching the shielding can.

the HEMT amplifier and IF isolator; (iii) a second sidelobe of the antenna beam was filed by the signal from hot/cold load due to absence of long shields.

The beam of the receiving antenna is formed by a few elements: (i) the printed double-dipole antenna; (ii) the back reflector attached to the chip and (iii) the elliptical lens described above. The antenna beam pattern, presented in figure 13, was mapped in front of the window of the test Dewar at the distance of 40 cm. The mapping principle is based on detection of a broad beam source, which is being translated in front of the cryostat in the plane perpendicular to the receiver beam axis. The level of the first-order sidelobe was found at about −16 dB with the beam width of 3.7 and 6.7° at the −3 dB and −10 dB levels respectively. The first minimum in the radiation pattern occurs at approximately 4.5°. This corresponds roughly to an $f/9.4$ beam with a waist size $w_0 \approx 3.6$ mm. The cross-polarization component as calculated and measured is approximately 20 dB below the co-polar level. The comparison with a reference mixer showed that complex LO circuitry located in the antenna–mixer has a minor effect on the antenna beam pattern which is in good agreement with the theoretical prediction [56, 57].

4.8. Balanced SIS mixer

To minimize the signal loss due to the integrated LO, the concept of a balanced SIS mixer has been developed [52]. This mixer contains two SIS junctions each connected to its own antenna while the LO current applied in series to the junctions via a microstrip coupler. No leak of the equal in-phase (balanced) signal is possible to the LO path. The problem of limited LO power is not so severe for the balanced mixer in spite of the fact that a twin-junction mixer has to consume at least twice as much power as a single-junction mixer. The absence of (or very low) coupling of the signal to the LO path allow us to use 100% of the power available from the FFO. The IF signal from such a mixer is obtained as a composition of two anti-phased signals from the two mixing junctions. We demonstrated that an integrated receiver with the balanced mixer can operate with noise temperature less than 100 K (see figure 12) [26] that is at the level of the best SIS receivers with a 'traditional' LO.

Since a single FFO can, in principle, serve a frequency range of about 250–700 GHz, a mixer with a correspondingly wide band is desired. Recently an ultra-wide range SIS mixer (400–700 GHz) has been demonstrated using a twin-junction double-dipole antenna configuration [55, 64]. We have considered the possibility of building a wide band integrated receiver using the advantage of a two-junction configuration of the balanced SIS mixer. However, it was found that, combining two IF signals in the balanced mixer, an additional rf circuit has to be used and the wide band properties of the twin-cell mixer would be eventually lost. The balanced mixer of the present design has a bandwidth of 80–100 GHz (measured by FTS) that is, however, essentially wider than that of the single-junction integrated receiver (see figure 12).

4.9. Towards phase locked integrated receiver

Recent results on phase locking of an FFO to an external reference oscillator have been used to develop the concept of an integrated receiver with phase locked loop [49, 62] presented schematically in figure 14. Following this concept the 350 GHz receiver chip containing a quasioptical SIS mixer, a phase locked flux-flow oscillator, a harmonic SIS mixer and a SIS multiplier as a source for the harmonic mixer (optional) has been designed, fabricated and pre-tested recently [62, 63]. The FFO has to be phase locked to the 35th harmonic of a 10 GHz synthesized source using custom-designed room temperature electronics with a PLL loop bandwidth of about 10 MHz.

The present state of development of the PLL integrated receiver is, so far, quite encouraging. The receiver contains well understood devices and can be tested in the nearest future for practical spectral radio astronomy in the frequency range 350–450 GHz. In this frequency range the Fiske steps of the Nb–AlO_x–Nb FFO are closely spaced and almost overlapping due to the finite slope and dispersion in the long Josephson tunnel junction [43]. The frequency gaps between the available LO bands (at subsequent FSs), where FFO phase locking is possible, do not exceed 5 GHz. There is a possibility of covering these gaps by a receiver by using a wide-band IF amplifier with wide enough

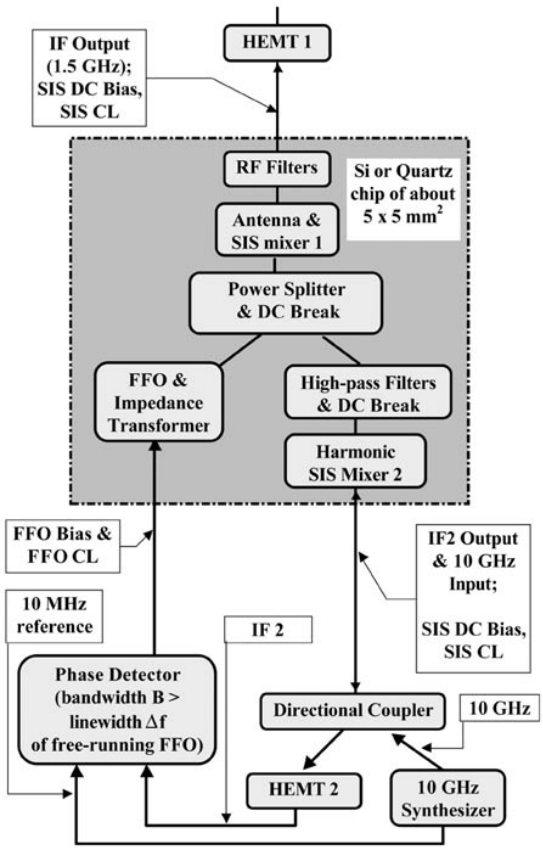

Figure 14. Block diagram of the proposed sub-millimetre all-superconducting phase locked single-chip integrated receiver [49]. The common FFO pumps two SIS mixers: one serves as the detector/mixer, and the other facilitates the phase locking of the FFO.

bandwidth (2–4 GHz) while the FFO is biased and locked on adjacent FSs, that will result in continuous frequency coverage.

5. Imaging array receiver

5.1. Array receiver design

A focal plane imaging array receiver has been designed using the fly's eye concept [26, 52, 53] whereby all nine pixels are identical and easily exchangeable integrated receiver units described above, each with individual antireflection coated elliptical silicon optics and individually controlled local oscillator (figure 15(a)). The pixels are arranged in two rows (4 + 5), as presented in figure 15(b), using honeycomb packaging resulting in an equal distance of about 13 mm between all adjacent units. The array block was mounted on the cold plate of a specially designed cryostat, as shown in figure 16, equipped with a resonant Mylar window (10 cm in diameter, 180 μm thick). Because of the large window size, a number of filters are used to reduce the heat (infrared) load on the LHe vessel: a 6 mm thick plate of Teflon at 80 K and a Zitex membrane at the 4.2 K stage. The shielding enclosure of the array is basically a scaled version of the one described above.

5.2. Test of array receiver

Only two channels were possible to monitor simultaneously during test of the array, because of a deficit of both space inside cryostat and coolable IF amplifiers. A DSB noise temperature measured for the array is presented in figure 12 by circles. A 3 dB bandwidth of about 15% can be estimated with the lowest noise temperature of about 150 K, which is somewhat higher than a typical DSB noise temperature of about 120 K measured in the test cryostat. This can be certainly associated with loss in the thick (non-resonant) infrared filter at 80 K. There are, however, a few other reasons for the noise temperature increase. Since the depth of the magnetic shield of the array has to be at least twice as large as the aperture of the opening, the output cable connecting the chip to the IF circulator, which is not allowed inside the shield, is about 40 cm long and introduces about 1 dB loss. It turns out also to be difficult to provide perfect cooling for the 50 Ω termination of the (shielded) circulator due to its design. All these restrictions and changes in the array cryostat arrangement caused the increase of the noise temperature of the IF channel and as a result the rise of the noise temperature of the complete receiver. It worth noting here that an integrated IF amplifier would be an ultimate solution for this problem.

Figure 17 presents data on antenna beams of two neighbouring pixels. Both beam patterns are, within the accuracy of the measurement, the same as measured in the qualification test. The separation of beams, indicated in figure 17, corresponds well to the mechanical position of pixels. No rf cross-talk within the array mount or cryostat has been found, unless a mirror-like obstacle is installed in front of the cryostat in a special experiment and some LO power can be directed (reflected) from one pixel to another.

6. SQUID amplifier

6.1. Motivations for SQUID amplifier

An rf amplifier, which can be integrated with or (at least) attached to an IF port of the SIS mixer or integrated receiver, is very attractive since it helps to avoid losses of the long cable and, possibly, circulator. A semiconductor IF amplifier 'integrated' into the fixture of the SIS mixer was reported, demonstrating quite encouraging results [65]. However, use of such an amplifier creates two distinctive problems: (i) heat of the amplifier (20 mW per stage typically) has to be terminated to the cold bath keeping the SIS structure cold and (ii) any variations of the output impedance of the SIS mixer have to be accepted by the amplifier (i.e. it has to be stable in a wide range of input impedance). The heat sinking is a known problem for quasi-optical mixers even without any amplifiers attached. Semiconductor amplifiers of balanced design are well known for their stable operation, but they produce twice as much heat. All these make an rf amplifier based on a dc SQUID (SQA) a natural choice for integration with a SIS mixer and, further, with an integrated receiver. The SQA has a number of crucial advantages over the traditional semiconductor IF amplifiers: ultra-low power consumption, small size and natural compatibility with any SIS based structure. This is why the study of an SQA is

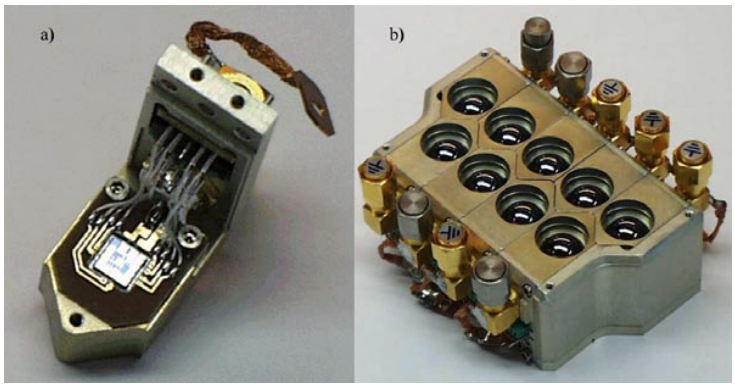

Figure 15. (a) Replaceable element of the nine-pixel imaging array. The unit is shown from the side of the receiver chip, which is mounted on the elliptical microwave lens and wire bonded to the printed circuit board. (b) Nine-pixel imaging array receiver block. Each pixel is an independent integrated receiver with its own internal local oscillator. The array mount is shown from the side of its input microwave lenses.

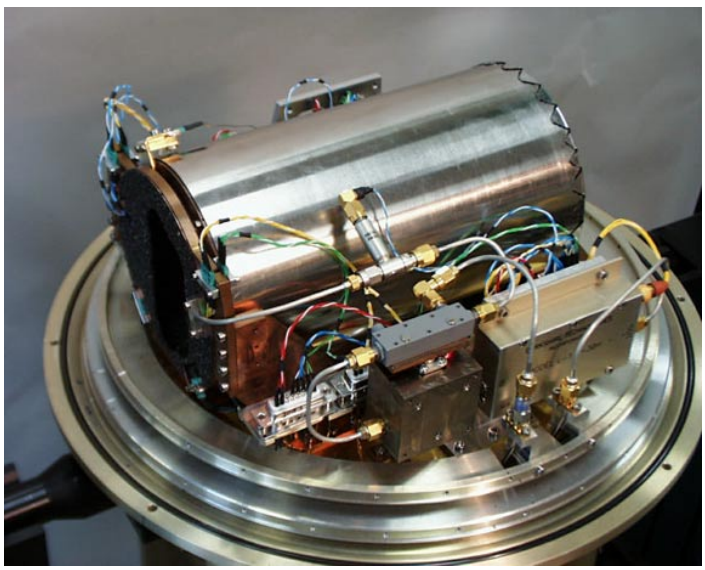

Figure 16. Open cryostat with nine-pixel imaging array mounted inside the cylindrical shielding can at 4.2 K. A low noise HEMT IF amplifier with magnetically shielded isolator and directional coupler are in the foreground.

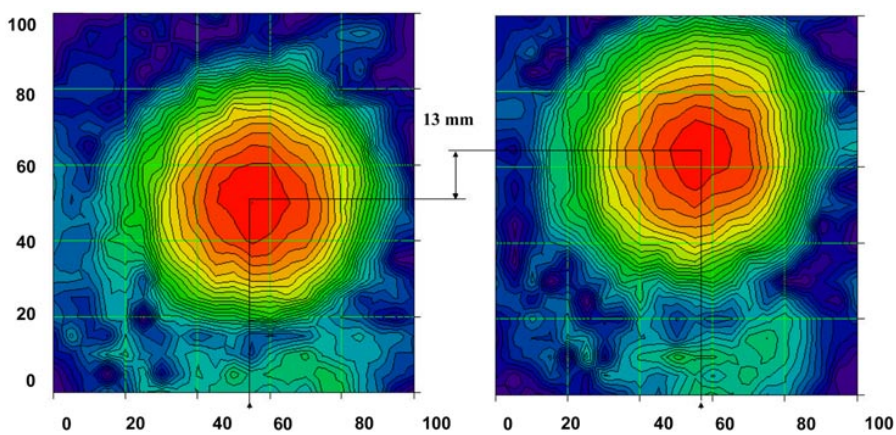

Figure 17. Antenna beam pattern for two adjacent pixels; contour steps are at 1 dB. Both axes present the linear shift of the irradiation source (in millimetres). The antenna beam is mapped at 470 GHz with the source in front of the test Dewar at the distance of 40 cm.

a logical step for further integration of superconducting rf devices, e.g. as a solution for IF noise, heat and space problems of the imaging array.

It has been shown by Muck *et al* [31] that RF amplifiers based on a niobium dc SQUID with resonant input circuit can achieve gain of about 18 dB and a noise temperature

in the range from 0.5 ± 0.3 K (at 80 MHz) to 3.0 ± 0.7 K (at 500 MHz). However for a real application (e.g. in radio astronomy) the instant bandwidth of at least 0.5–1 GHz is desired. To reach this value, an attempt [32–34] was made to design an SQA with higher central frequency (4 GHz) while its bandwidth, determined by a resonant input coil (of order of 10%), would be sufficiently wide.

6.2. Design of SQA

The concept described in [32–34] follows the principle of resonant coupling of a microwave signal to the SQUID loop. To avoid parasitic resonant phenomena in the SQUID, that is the usual limit for operation frequency, a new design of the coupling circuit has been developed using extensive scale modelling. The modelling included study of an optimal shape of both the SQUID washer and the input coil as well as the place of connection of capacitors and other rf elements.

Figure 18 [32] presents a partial view of the SQA chip and includes the coupling circuit. The double-washer SQUID has two square holes and two four-turn input coils placed inside the holes. This configuration provides the lowest possible capacitance between the input coils and the washer. The input coils are connected in series. Most of the parasitic capacitance to the washer arises, according to our estimate, from the underlying lines providing connection of the two input coils in series. The capacitors C_1, C_2 are chosen to tune a resonance of the input coil at the signal frequency $f_S \approx 3.7$ GHz. The coupling of the signal was measured with a scale model of the circuit as a ratio of rf power applied to the input coil of the resonant transformer and rf power detected across the SQUID washer. Both the source and the detector have impedance of 50 Ω. A typical loss of a few dB was found. The analysis of coupling against frequency was made up to 50 GHz (of scaled frequency). No presence of unwanted resonant phenomena was found.

Since the output load of the SQA is connected in parallel to junctions of the SQUID, special care is taken to avoid possible disturbance of the SQUID IVC due to unknown impedance of the output connection. In other words, the condition of an open circuit within a wide range of Josephson frequency (bias voltage) has been provided. Two integrated low pass filters with central frequency of about 50 GHz are employed. Such a filter transmits the dc bias and the signal at f_S, but prevents the Josephson current $f_J \gg f_S$, from leaking out of the SQUID. To adjust the magnetic bias, the common part of the two-loop washer of the SQUID is used as an integrated control line. It is important to note that some signal leak through the SQA can be predicted as a result of inductive coupling between the input coil and the washer of the SQUID (exactly as tested for mutual coupling). To prevent ghost output signals, the washer is short-circuited at the signal frequency with the above mentioned output filters connected to each junction. We call this configuration a balanced output SQUID amplifier. The main parameters of the SQA are listed in table 1 [32, 33].

To demonstrate the general feasibility of the approach, the SQA unit has been designed and tested (see figure 19).

Table 1. Parameters of SQUID-based RF amplifier [33].

Parameter	Experimental data
SQUID inductance	$L_{SQA} \approx 70$ pH
Coupling coefficient	$k^2 \approx 0.6$
Area of SIS junction	$A_{SIS} \approx 1.0\ \mu\text{m}^2$
Capacitance of SIS junction	$C_{SIS} \approx 0.1$ pF
Critical current	$I_c \approx 21\ \mu$A
McCumber parameter	$\beta_c \approx 0.1$
Inductance parameter β_L	$\beta_L \approx 1$
Shunt resistance per junction	$R_{sh} \approx 8\ \Omega$
Time constant of the SQUID	$\tau = L_{SQA}/R_{sh} \approx 10^{-10}$ s
Inductance of input coil	$L_{coil} \approx 3$ nH
Input circuit capacitance	$C_1 = C_2 \approx 1$ pF
Size of two-stage SQA chip	$6 \times 6\ \text{mm}^2$
Central operating frequency	$f_c \approx 3.7$ GHz
Dynamic resistance at bias point	$R_d \approx 23\ \Omega$
Voltage at the bias point	$V_b \approx 18\ \mu$V
Power gain per stage	$G_1(\text{max}) \approx 11.0 \pm 1.0$ dB
Gain bandwidth	$\Delta f_{3\,dB} \approx 210$ MHz
Noise temperature	$T_n(\text{min}) \approx 9.0 \pm 1.0$ K
Intrinsic flux noise	$S\Phi^{1/2}(\text{min}) \approx 0.7\ \mu\Phi_0\ \text{Hz}^{-1/2}$

This stand-alone unit contains a two-stage SQA amplifier chip and a launcher system that couples the chip to standard SMA connectors. It is possible to measure each stage separately via the intermediate SMA connector.

6.3. Test of SQA

Noise temperature and gain of the SQA have been measured [33, 34] with a room temperature noise source and calibrated cold attenuators. The effect of saturation was found to be most pronounced for the two-stage configuration that can, in principle, be accepted for radio astronomy (very weak signals), but it is certainly not good for more general applications. A narrow-band filter (40 MHz) was used then at the SQA input in order to obtain reliable data on the noise temperature and gain. To increase the saturation level of the SQA, the feasibility of a negative feedback loop was demonstrated recently by Prokopenko *et al* [34] with saturation level improvement to about 100 K. The following parameters have been measured for the single-stage device at 3.65 GHz in the feedback mode: gain of (11.0 ± 1.0) dB, 3 dB bandwidth of about 300 MHz and noise temperature (9.0 ± 1.0) K that corresponds to the flux noise $S_\Phi^{1/2} \approx 0.7\ \mu\Phi_0\ \text{Hz}^{-1/2}$ and energy sensitivity $\varepsilon_i \approx 160\hbar(2.0 \times 10^{-32}\ \text{J Hz}^{-1})$. The detailed data on gain and noise temperature of the experimental unit are presented in figure 20 [34].

7. Superconducting digital correlator

A new concept of a superconducting digital correlator based on ultrafast RSFQ elements [36] was suggested recently [35, 66, 67] and successfully realized [37, 68, 69]. The proposed device is a one-bit (or so-called *sign*) autocorrelator, which contains a one-bit quantizer of an input signal. The correlator's hardware can be divided into two parts: a delay line with multiplication and accumulator stages. The inherent clock frequency of elementary RSFQ cells up to 370 GHz has been achieved [70], that is a unique result. Extremely low

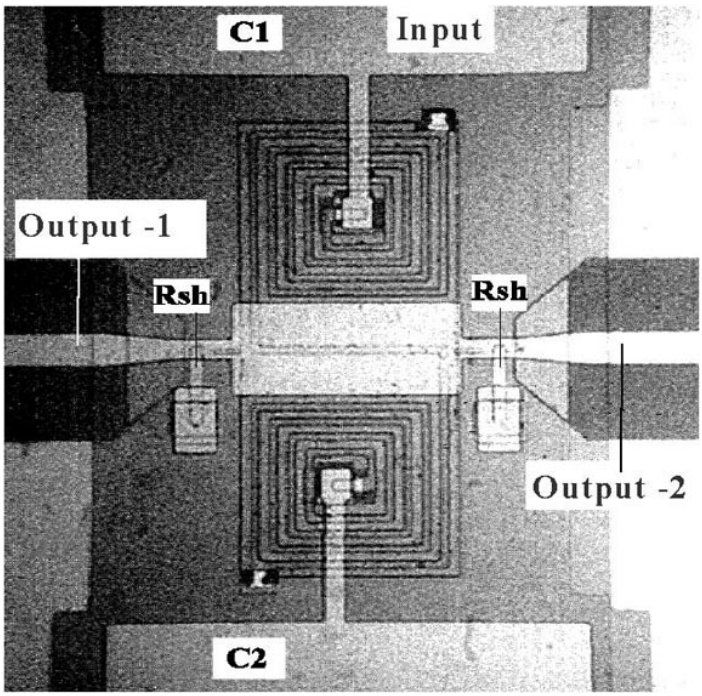

Figure 18. Partial view of chip of balanced SQA [32]. Two capacitors C_1 and C_2 and two series input coils (inside holes of the SQUID washer) are tuned at about 4 GHz. The wide strip in the centre is a superconducting control line for magnetic bias of the SQUID. Two outputs, connected to each of two shunted SIS junctions, provide rejection of the common mode. Output filters are out of the field of view.

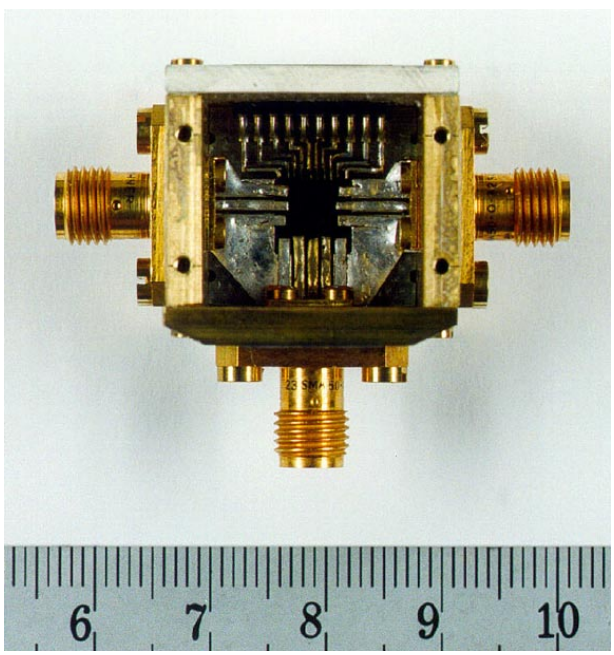

Figure 19. Experimental SQA unit with launcher system providing effective rf coupling between chip and standard SMA connectors [34].

total power dissipation can also be achieved (including the dissipation in the biasing resistors) due to the low signal level and the very fast switching time of the superconducting gates. The power dissipation of about 1 μW/gate extends the device integration limit (set usually by cooling problems) up to 10^6 devices per cm^2 that is far beyond those of semiconductor electronics. Superconducting microstrip lines have very low attenuation and dispersion up to 1 THz that is a favourable feature of Josephson junction technology. All basic elements of the proposed correlator have been developed and tested earlier, so the feasibility of their combination looks rather probable.

A fully integrated all-digital one-bit RSFQ autocorrelator for sub-mm spectrometry application has been designed and successfully tested at frequencies up to 11 GHz [37]. The 16-channel device has been completed with a 16×9 array of binary counters, on-chip double-oversampling quantizer and on-chip clock generator. The total number of Josephson junctions in the design was 1672 with an estimated total power dissipation of less than 0.1 mW. For high-speed testing of the device, a specialized 16-channel room temperature interface has been developed [37], which is capable of using output an rate of real time data acquisition of 16 Mbps (per channel). The experimental chips were fabricated at Hypres using their standard 3.5 μm Nb–AlO_x–Nb process with current density of about 1 kA cm^{-2}. The concept of a 128-channel autocorrelator system employing eight independent identical chips was proposed in [37] with an estimated Josephson junction count of about 2500 per chip. This integration level is well reachable for the present-day fabrication technology. An estimation for the main parameters of a 1024-channel RSFQ correlator is presented in table 2.

8. Conclusions

The combination of narrow linewidth and wide band tuneability makes the FFO a perfect on-chip local oscillator for an integrated sub-mm receiver for spectral radio astronomy and aeronomy applications. Implementation of

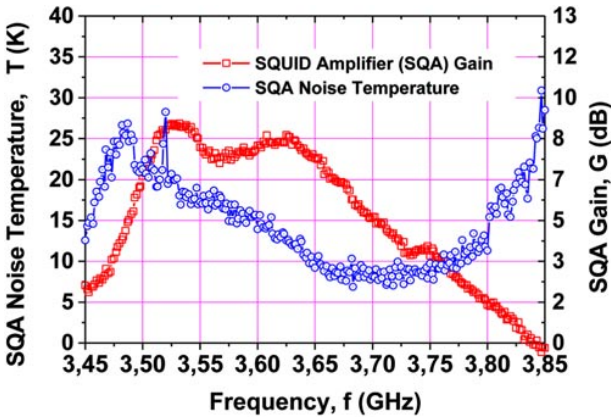

Figure 20. Noise temperature and gain measured for a single-stage dc SQUID based rf amplifier [34].

Table 2. Parameters of RSFQ correlator.

Frequency band	2 GHz
Frequency resolution	about 2 MHz
Clock frequency (at double oversampling)	8 GHz
Total number of channels	1024
Number of accumulator stages	22
Result representation code	16 bit
Readout frequency	> 16 kbit s^{-1}
Total number of Josephson junctions	$\approx$100 000
Total power dissipation	$\sim$1 mW

the single-chip superconducting integrated receiver (SIR) for new radio-astronomy projects based on a multi-receiver approach (e.g. ALMA) is especially advantageous due to the lower price and better serviceability of the single-chip SIR as compared to a conventional SIS receiver with a Gunn oscillator and multipliers. It is important to note that ultimate performance of the quasi-optical SIR is basically the same as for waveguide SIS receivers in the frequency range of 400–600 GHz while the wide band tuneability and convenience of electronic control of the local oscillator (FFO) offer extra advantages of the SIR over a regular SIS receiver. The data given above demonstrate electronic control of the frequency and power of the FFO along with the possibility of narrowing the linewidth of a Josephson oscillator using an external PLL system, provided that the PLL bandwidth is larger than the intrinsic linewidth of the free-running oscillator.

The integrated receivers fabricated on the base of a niobium trilayer Nb/AlO_x/Nb are proven to be useful within the frequency range 100–700 GHz showing noise temperatures better than 1 K GHz^{-1} that is close to the performance of 'traditional' SIS receivers with external LOs. The antenna beam properties obtained for the integrated receiver are satisfactory for use on a real telescope. The concept of the PLL integrated receiver is at the stage of intensive experimental study. The imaging array receiver based on nine integrated receiver pixels employing elliptical silicon optics is developed and tested showing no essential degradation of the pixel performance. An rf amplifier on the base of a dc SQUID is developed and tested at 4 GHz that is the highest frequency among dc SQUID amplifiers tested up to date. A device of this type can be an effective IF solution for a multi-channel imaging array receiver.

The integration of SIS mixer, planar antenna and FFO together with the circuits for analogue to digital conversion and real time data processing provides an excellent opportunity for the realization of a modular satellite cryogenic receiver. This receiver will have according to our estimations unique parameters: noise temperature only ten times above the quantum limit at frequencies possibly as high as 700 GHz, spectral resolution about 2 MHz over a 2 GHz bandwidth, low power dissipation and high reliability.

Acknowledgments

The work was supported in part by the Russian SSP 'Superconductivity', INTAS project 97-1712, ISTC project No 1199, the Nederlandse Organisatie voor Wetenschappelijk Onderzoek (NWO) grant and ESA TRP contract 11/653/95/NL/PB/SC. The authors deeply appreciate the participation in the development and study of the integrated receiver of all members of the large international team, especially Andrey Baryshev, Andrey Ermakov, Lyudmila Filippenko, Pavel Dmitriev, Petri Lehikoinen, Willem Luinge, Jesper Mygind, Georgy Prokopenko and Vladimir Vaks. The authors thank Thijs de Graauw, Herman van de Stadt, Paul R Wesselius, Nick Whyborn, Peter de Maaght, Martin van der Vorst and Wolfgang Wild for fruitful and stimulating discussions as well as H Golstein, S Kikken, H Smit, J Evers and D Van Nguyen for help in the experiment.

References

[1] Tucker J R and Feldman M J 1985 *Rev. Mod. Phys.* **4** 1055–113
[2] Blondel R and Tong C E 1992 *Proc. IEEE* **80** 1702–20
[3] Shitov S V, Koshelets V P, Kovtonyuk S A, Ermakov An B, Whyborn N D and Lindstrom C-O 1991 *Supercond. Sci. Technol.* **4** 406–8
[4] Karpov A, Blondel J, Voss M and Gundlach K H 1995 *IEEE Trans. Appl. Supercond.* **5** 3304–7
[5] Zmuidzinas J and LeDuc H G 1992 *IEEE Trans. Microwave Theory Tech.* **40** 1797–804
Zmuidzinas J, Ugras N G, Miller D, Gaidis M, LeDuc H G and Stern J A 1995 *IEEE Trans. Appl. Supercond.* **5** 3053–6
[6] Gaidis M C, Leduc H G, Mei Bin, Miller D, Stern J A and Zmuidzinas J 1996 *IEEE Trans. Microwave Theory Tech.* **44** 1130–9
[7] Han S, Bi B, Zhang W and Lukens J E 1994 *Appl. Phys. Lett.* **64** 1424–6
[8] Kiryu S, Zhang W, Han S, Deus S and Lukens J E 1997 *IEEE Trans. Appl. Supercond.* **7** 3107–10
[9] Deus S and Kiryu S 1999 *IEEE Trans. Appl. Supercond.* **9** 4325–8
[10] Booij P A A and Benz S P 1996 *Appl. Phys. Lett.* **68** 3799–801
[11] Kawakami A and Wang Z 1998 *IEICE Trans. Electron.* **61** 1595–600
[12] Kawakami A, Uzawa Y and Wang Z 1999 *IEEE Trans. Appl. Supercond.* **9** 4554–7
[13] van der Zant H S J and Orlando T P 1994 *J. Appl. Phys.* **76** 7606–12
[14] Wengler M J, Guan B and Track B 1995 *IEEE Trans. Microwave Theory Tech.* **43** 984–8
[15] Booij P A A and Benz S P 1994 *Appl. Phys. Lett.* **64** 2163–5

[16] Caputo P, Ustinov A V, Lin N C H and Yukon S P 1999 *IEEE Trans. Appl. Supercond.* **9** 4538–41

[17] Oppenlinder J, Guttinger W, Traeuble T, Kerk M and Doderer T 1999 *IEEE Trans. Appl. Supercond.* **9** 4337–40

[18] Barbara P, Cawthorne A B, Shitov S V and Lobb C J 1999 *Phys. Rev. Lett.* **82** 1963–5

[19] Koshelets V P, Shitov S V, Shchukin A V, Baryshev A M, Filippenko L V, Fisher G M and Mygind J 1993 *Appl. Phys. Lett.* **63** 3218–20

[20] Nagatsuma T, Enpuku K, Irie F and Yoshida K 1983 *J. Appl. Phys.* **54** 3302–9
Nagatsuma T, Enpuku K, Irie F and Yoshida K 1984 *J. Appl. Phys.* **56** 3284
Nagatsuma T, Enpuku K, Irie F and Yoshida K 1985 *J. Appl. Phys.* **58** 441
Nagatsuma T, Enpuku K, Irie F and Yoshida K 1988 *J. Appl. Phys.* **63** 1130

[21] Mygind J, Koshelets V P, Shchukin A V, Shitov S V and Lapytskaya I L 1995 *IEEE Trans. Appl. Supercond.* **5** 2951–4

[22] Koshelets V P, Shitov S V, Baryshev A M, Lapytskaya I L, Filippenko L V, van de Stadt H, Mess J, Schaeffer H and de Graauw T 1995 *IEEE Trans. Appl. Supercond.* **5** 3057–60

[23] Koshelets V P, Shchukin A V, Shitov S V and Filippenko L V 1993 *IEEE Trans. Appl. Supercond.* **3** 2524–7

[24] Koshelets V P, Shitov S V, Filippenko L V, Baryshev A M, Golstein H, de Graauw T, Luinge W, Schaeffer H and van de Stadt H 1996 *Appl. Phys. Lett.* **68** 1273–5

[25] Koshelets V P *et al* 1996 *Proc. 30th ESLAB Symp.* (ESTEC) pp 193–202

[26] Shitov S V, Ermakov A B, Filippenko L V, Koshelets V P, Baryshev A B, Luinge W and Gao J-R, 1999 *IEEE Trans. Appl. Supercond.* **9** 3773–6

[27] Koshelets V P, Shitov S V, Shchukin A V, Filippenko L V and Mygind J 1996 *Appl. Phys. Lett.* **69** 699–701

[28] Koshelets V P, Shitov S V, Filippenko L V, Vaks V L, Mygind J, Baryshev A B, Luinge W and Whyborn N 2000 *Rev. Sci. Instrum.* **71** 289–93

[29] Hilbert C and Clarke J 1985 *J. Low Temp. Phys.* **61** 263–81

[30] Tarasov M A, Prokopenko G V, Koshelets V P, Lapytskaya I L and Filippenko L V 1995 *IEEE Trans. Appl. Supercond.* **5** 3226–9

[31] Muck M, Andre M-O and Clarke J 1998 *Appl. Phys. Lett.* **72** 2885–7

[32] Prokopenko G P, Shitov S V, Koshelets V P, Balashov D V and Mygind J 1997 *IEEE Trans. Appl. Supercond.* **7** 3496–99

[33] Prokopenko G V, Balashov D V, Shitov S V, Koshelets V P and Mygind J 1999 *IEEE Trans. Appl. Supercond.* **9** 2902–5

[34] Prokopenko G V, Balashov D V, Shitov S V, Koshelets V P and Mygind J 1999 *EUCAS'99 (Barcelona)* report 6–80

[35] Goldobin E B, Litskevitch P G and Koshelets V P 1995 *Extended Abstracts ISEC'95 (Nagoya)* pp 231–3

[36] Likharev K K and Semenov V K 1991 *IEEE Trans. Appl. Supercond.* **1** 3–28

[37] Rylyakov A V, Schneider D F and Polyakov Yu A 1999 *IEEE Trans. Appl. Supercond.* **9** 3623–6

[38] Kohjiro S and Shoji A 1999 *EUCAS'99 (Barcelona)* report 6–103

[39] Koshelets V P, Shitov S V, Filippenko L V, Baryshev A B, Luinge W, Golstein H, van de Stadt H, Gao J-R and de Graauw T 1997 *IEEE Trans. Appl. Supercond.* **7** 3589–92

[40] Koshelets V P, Shitov S V, Shchukin A V, Filippenko L V, Mygind J and Ustinov A V 1997 *Phys. Rev.* B **56** 5572–7

[41] Lee G S 1991 *IEEE Trans. Appl. Supercond.* **3** 121–7
Thyssen N, Ustinov A V, Kohlstedt H, Pagano S, Caputo J G and Flytzanis N 1995 *IEEE Trans. Appl. Supercond.* **5** 2965–8

[42] Ustinov A V, Kohlstedt H and Henne P 1996 *Phys. Rev. Lett.* **77** 3617–20

[43] Cirillo M, Gronbech-Jensen N, Samuelsen M R, Salerno M and Verona Rinati G 1998 *Phys. Rev.* B **58** 12377–84

[44] Hasselberg L-E, Levinsen M T and Samuelsen M R 1974 *Phys. Rev.* B **9** 3757–65

[45] Ustinov A V, Doderer T, Huebener R P, Mygind J, Oboznov V A and Pedersen N F 1993 *IEEE Trans. Appl. Supercond.* **3** 2287–94

[46] Koshelets V P, Shchukin A V, Lapytskaya I L and Mygind J 1995 *Phys. Rev.* B **51** 6536–41

[47] Zhang Y M, Winkler D and Claeson T 1993 *Appl. Phys. Lett.* **62** 3195–7

[48] Muller U and Jacobs K 1999 *Proc. 10th Int. Symp. on Space Terahertz Technology (Charlottesville)* pp 13–28

[49] Koshelets V P, Shitov S V, Shchukin A V, Filippenko L V, Dmitriev P N, Vaks V L, Mygind J, Baryshev A B, Luinge W and Golstein H 1999 *IEEE Trans. Appl. Supercond.* **9** 4133–6

[50] Stephen M J 1969 *Phys. Rev.* **182** 531–8

[51] Likharev K K 1986 *Dynamics of Josephson Junctions and Circuits* (London: Gordon and Breach)

[52] Shitov S V *et al* 1997 *Proc. 8th Int. Symp. on Space Terahertz Technology* pp 281–90

[53] Shitov S V, Ermakov A B, Filippenko L V, Koshelets V P, Luinge W, Baryshev A M, Gao J-R and Lehikoinen P 1998 *Proc. 9th Int. Symp. on Space Terahertz Technology* pp 263–72

[54] Dierichs M M T M, Panhuyzen R A, Honingh C E, de Boer M J and Klapwijk T M 1993 *Appl. Phys. Lett.* **62** 774–6

[55] Skalare A, de Graauw T and van de Stadt H 1991 *Microwave Opt. Technol. Lett.* **4** 9–12

[56] van der Vorst M J M, de Maagt P J I and Herben M H A J 1996 *Proc. the Int. Symp. on Antennas, JINA '96* pp 511–5

[57] van der Vorst M J M, de Maagt P J I and Herben M H A J 1999 *IEEE Microwave Theory and Tech.* **47** 1696–705

[58] Rebeiz G M 1992 *Proc. IEEE* **80** 1749–70

[59] Neman H S and Davis K L 1982 *J. Appl. Phys.* **53** 7026

[60] Shitov S V *et al* 1994 *Proc. 19th Int. Conf. on Infrared and Millimeter Waves (Sendai)* pp 122–3

[61] Baryshev A B, Luinge W, Koshelets V P, Shitov S V and Klapwijk T M 1998 unpublished

[62] Shitov S V, Koshelets V P, Filippenko L V, Dmitriev P N, Baryshev A M, Luinge W and Gao J-R 1999 *Proc. 10th Int. Symp. on Space Terahertz Technology (Charlottesville)* pp 447–58

[63] Shitov S V, Koshelets V P, Filippenko L V, Dmitriev P N, Vaks V L, Baryshev A M, Luinge W, Whyborn N D and Gao J-R 1999 *EUCAS'99 (Barcelona)* report 6–100

[64] Shitov S V, Baryshev A M, Koshelets V P, Gao J-R, Jegers J, Luinge W, van de Stadt H and de Graauw T 1996 *Proc. 7th Int. Symp. on Space Terahertz Technology (Charlottesville)* pp 525–35

[65] Padin S, Woody D P, Stern J A, LeDuc H G, Blundel R, Tong C-Y E and Pospiezalski M W 1996 *IEEE Trans. Microwave Theory Tech.* **44** 987–90

[66] Kidiyarova-Shevchenko A Yu and Litskevitch P G 1996 *Nuclear Physics Institute Moscow State University Preprint* 96-21/428

[67] Litskevitch P G and Kidiyarova-Shevchenko A Yu 1997 *Extended Abstracts 6th Int. Superconductive Electronics Conf. ISEC-97* vol 2, pp 356–8

[68] Rylyakov A V 1997 *IEEE Trans. Appl. Supercond.* **7** 2709–12

[69] Rylyakov A V and Pololonsky S V 1998 *IEEE Trans. Appl. Supercond.* **8** 14–9

[70] Bunyk P I, Oliva A, Semenov V K, Blushan M, Likharev K K, Lukens J E, Ketchen M B and Mallison W H 1995 *Appl. Phys. Lett.* **66** 646–8